



**HAL**  
open science

## Mechanical properties of membranes composed of gel-phase or fluid-phase phospholipids probed on liposomes by atomic force spectroscopy

Oumaima Et Thakafy, N. Delorme, Cedric Gaillard, Cristelle Mériadec, Franck Artzner, Christelle Lopez, Fanny Guyomarc'H

### ► To cite this version:

Oumaima Et Thakafy, N. Delorme, Cedric Gaillard, Cristelle Mériadec, Franck Artzner, et al.. Mechanical properties of membranes composed of gel-phase or fluid-phase phospholipids probed on liposomes by atomic force spectroscopy. *Langmuir*, 2017, 33 (21), pp.5117-5126. 10.1021/acs.langmuir.7b00363 . hal-01529481

**HAL Id: hal-01529481**

**<https://hal.science/hal-01529481>**

Submitted on 13 Jul 2017

**HAL** is a multi-disciplinary open access archive for the deposit and dissemination of scientific research documents, whether they are published or not. The documents may come from teaching and research institutions in France or abroad, or from public or private research centers.

L'archive ouverte pluridisciplinaire **HAL**, est destinée au dépôt et à la diffusion de documents scientifiques de niveau recherche, publiés ou non, émanant des établissements d'enseignement et de recherche français ou étrangers, des laboratoires publics ou privés.



Distributed under a Creative Commons Attribution - ShareAlike 4.0 International License

1  
2  
3 1 **Mechanical properties of membranes composed of gel-phase or fluid-phase**  
4  
5 2 **phospholipids probed on liposomes by atomic force spectroscopy**  
6  
7

8  
9 3  
10  
11 4 Oumaima ET-THAKAFY<sup>‡</sup>, Nicolas DELORME<sup>†</sup>, Cédric GAILLARD<sup>||</sup>, Cristelle  
12  
13 5 MERIADEC<sup>§</sup>, Franck ARTZNER<sup>§</sup>, Christelle LOPEZ<sup>‡</sup>, Fanny GUYOMARC'H<sup>‡\*</sup>  
14  
15  
16  
17 6

18  
19  
20 7 <sup>‡</sup> STLO, INRA, Agrocampus Ouest, 35000, Rennes, France  
21

22 8 <sup>||</sup> UR BIA 1268 Biopolymères Interactions Assemblages, INRA, 44316 Nantes, France  
23

24  
25 9 <sup>§</sup>Institut de Physique de Rennes, UMR 6251, CNRS, Université de Rennes 1, 263 Av. Général  
26  
27 10 Leclerc, 35042 Rennes, France  
28

29  
30 11 <sup>†</sup> UMR CNRS 6283 Institut des Molécules et Matériaux du Mans, Université du Maine,  
31  
32 12 Université Bretagne-Loire, 72000 Le Mans, France  
33  
34

35  
36 13 \*Corresponding author: Fanny Guyomarc'h  
37

38  
39 14 Key words: small unilamellar vesicle; Phase state; Bending modulus; Young's modulus;  
40  
41 15 Atomic force microscopy  
42  
43

44 16 **Abstract**  
45

46  
47 17 In many liposome applications, the nanomechanical properties of the membrane envelope are  
48  
49 18 essential to ensure e.g. physical stability, protection or penetration into tissues. Of all factors,  
50  
51 19 the lipid composition and its phase behavior are susceptible to tune the mechanical properties  
52  
53 20 of membranes. To investigate this, small unilamellar vesicles (SUV; diameter <200 nm),  
54  
55  
56  
57  
58  
59  
60

1  
2  
3 21 referred to as liposomes, were produced using either the unsaturated 1,2-dioleoyl-sn-glycero-  
4  
5 22 3-phosphocholine (DOPC) or the saturated 1,2-dipalmitoyl-sn-glycero-3-phosphocholine  
6  
7  
8 23 (DPPC) in aqueous buffer at pH 6.7. The respective melting temperatures of these  
9  
10  
11 24 phospholipids were -20°C and 41°C. X-ray diffraction analysis confirmed that at 20°C DOPC  
12  
13  
14 25 was in the fluid phase and DPPC was in the gel phase. After adsorption of the liposomes onto  
15  
16  
17 26 flat silicon substrates, atomic force microscopy (AFM) was used to image and probe the  
18  
19  
20 27 mechanical properties of the liposome membrane. The resulting force-distance curves were  
21  
22 28 treated using an analytical model based on the shell theory to yield the Young's modulus ( $E$ )  
23  
24  
25 29 and the bending rigidity ( $k_C$ ) of the curved membranes. The mechanical investigation showed  
26  
27  
28 30 that DPPC membranes were much stiffer ( $E = 116 \pm 45$  MPa) than those of DOPC ( $E = 13 \pm$   
29  
30 31 9 MPa) at 20°C. The study demonstrates that the employed methodology allows  
32  
33 32 discrimination of the respective properties of gel- or fluid-phase membranes when in the  
34  
35  
36 33 shape of liposomes. It opens perspectives to map the mechanical properties of liposomes  
37  
38  
39 34 containing both fluid and gel phases or of biological systems.

## 35 I. INTRODUCTION

36 In the recent years, small unilamellar vesicles of phospholipids ( $< \mu\text{m}$  diameter) have gained  
37  
38 37 increasing interest in various liposome technologies, e.g. as drug delivery systems in  
39  
40 38 pharmacy or as protective cargo capsules for cosmetics, nutraceuticals or for food design<sup>1,2</sup>.  
41  
42  
43 39 They are also interesting models to investigate and possibly control *in vivo* biological  
44  
45  
46 40 signaling mechanisms involving extracellular vesicles such as the so-called exosomes<sup>3,4</sup>. The  
47  
48  
49  
50  
51  
52  
53  
54  
55  
56  
57  
58  
59  
60

1  
2  
3 41 composition of the phospholipids, i.e. the acyl chains' saturation/unsaturation and length,  
4  
5 42 impacts their phase state in the liposomes at ambient temperatures<sup>5</sup>. This, in turn, is likely to  
6  
7  
8 43 affect the mechanical properties of the liposomes, which are of paramount importance for  
9  
10  
11 44 these applications. Mechanical properties direct the stability, size, shape and fusion of the  
12  
13  
14 45 liposomes<sup>6-8</sup> as well as the membrane fluidity/rigidity or permeability and hence their loading  
15  
16  
17 46 capacity or their ability to penetrate tissues<sup>9-13</sup>. For example, the permeability of various  
18  
19  
20 47 saturated polar lipid membranes to glucose strongly increases as the lipid undergoes gel-to-  
21  
22  
23 48 liquid disordered ( $l_d$ ) phase transition<sup>14</sup>. As another example, milk sphingomyelin exhibited  
24  
25  
26 49 maximum permeability at temperatures where gel-to- $l_d$  phase transition occurs<sup>13</sup>. This has  
27  
28  
29 50 important consequences on the formulation and design of liposomes, as the desirable  
30  
31  
32 51 mechanical properties will differ depending on the application and temperature, e.g. storage at  
33  
34  
35 52 ambient temperature, transdermal delivery of drugs, etc. Experimental techniques to measure  
36  
37  
38 53 the mechanical properties of liposomes, such as the pipette aspiration technique, osmotic or  
39  
40  
41 54 mechanical compression, shear-induced or optical tweezers deformation<sup>7</sup> are often designed  
42  
43  
44 55 for large objects of the  $\mu\text{m}$  length scale. For liposomes at the nanoscale, such as small  
45  
46  
47 56 unilamellar vesicles, indentation measurement using atomic force microscopy (AFM) has  
48  
49  
50 57 proven a valuable and sensitive approach<sup>15-20</sup>. The liposomes, adsorbed onto a flat substrate,  
51  
52  
53 58 are indented by the AFM with low penetration distances (i.e. the order of magnitude of the  
54  
55  
56 59 membrane thickness) and at as low force values as down to the pN. The major advantage of  
57  
58  
59 60 AFM over a nano-indenter is also its imaging capacity, which allows to locate liposomes and  
60

1  
2  
3 61 to indent them centrally, even though not perfectly normally<sup>16</sup>. In a pioneering study, Laney et  
4  
5 62 al.<sup>17</sup> extracted synaptic liposomes (~110 nm diameter) from the electric organ of the electric  
6  
7  
8 63 ray *Torpedo californica*, immobilized them by adsorption onto mica and measured elastic  
9  
10  
11 64 moduli values in the range 0.2 – 1.3 MPa. Liang et al.<sup>19,21,22</sup> followed the same approach on  
12  
13  
14 65 small (40-160 nm) liposomes of egg phosphatidylcholine (mainly  
15  
16  
17 66 stearyloleoylphosphatidylcholine, SOPC) and found that the elastic modulus increased with  
18  
19  
20 67 the addition of up to 50 mol % cholesterol from ~2 to 13 MPa. However, these authors used  
21  
22  
23 68 an adaptation of the Hertz model for their calculations that assumed the liposomes to be  
24  
25  
26 69 homogeneous filled spheres. By implementing the shell deformation theory, Delorme and  
27  
28 70 Fery<sup>16</sup> obtained higher elasticity values of ~110 MPa by indenting DPPC  
29  
30  
31 71 (dipalmitoylphosphatidylcholine) and proposed that the Hertz model underestimated the  
32  
33  
34 72 mechanical properties of the liposomes. However, due to its mono-unsaturation, egg PC has a  
35  
36  
37 73 melting temperature ( $T_m$ ) of -15°C and is therefore in the  $l_d$  or liquid crystalline ( $L\alpha$ ) phase at  
38  
39  
40 74 20°C, while the fully saturated DPPC is in the gel or solid-ordered ( $s_o$ ) phase ( $T_m$  =  
41  
42 75 41.7°C)<sup>22,23</sup>. Therefore, it is yet to assess whether the AFM indentation measurement  
43  
44  
45 76 combined with the shell theory interpretation is sensitive enough to discriminate liposomes  
46  
47  
48 77 with presumably different mechanical properties of their membranes, e.g. by comparing  
49  
50  
51 78 saturated and unsaturated phospholipids in different physical phases at 20°C.  
52  
53  
54 79 When the membranes are spread as two-dimensional supported lipid bilayers (SLBs),  
55  
56 80 measurement of the rupture force of membranes using AFM indentation has proven to fully  
57  
58  
59  
60

1  
2  
3 81 resolve mechanical differences between phospholipids with various chain lengths, saturation  
4  
5 82 degrees or head groups<sup>24</sup>. However, calculation of the SLBs' effective elasticity using  
6  
7  
8 83 indentation of the membrane and the Hertz model requires careful and narrow experimental  
9  
10  
11 84 conditions not to be affected by the support<sup>25</sup>. Furthermore, direct measurement on small  
12  
13  
14 85 liposomes would encompass possible curvature effects. Indeed, their high membrane  
15  
16  
17 86 curvature may affect their mechanical properties, as lateral intermolecular distances and  
18  
19  
20 87 forces vary across the bilayer's thickness<sup>26,27</sup>. However, indentation measurements on 3D  
21  
22  
23 88 vesicles may be either impossible<sup>28</sup>, require high deformation of the objects<sup>19</sup> or somewhat  
24  
25  
26 89 depend on the composition of the internal medium, if different from the surrounding  
27  
28  
29 90 medium<sup>29</sup>. For these reasons, there is interest to assess indentation measurement of the  
30  
31  
32 91 mechanical properties of membranes directly on volumetric objects such as liposomes.  
33  
34 92 In the present study, the respective elasticities and bending rigidities of membranes of either  
35  
36  
37 93 the unsaturated phospholipid dioleoylphosphatidylcholine (DOPC) or the saturated  
38  
39  
40 94 phospholipid dipalmitoylphosphatidylcholine (DPPC) as shaped in the form of liposomes,  
41  
42  
43 95 were measured at 20°C using AFM indentation and the shell theory. The results were  
44  
45  
46 96 discussed in light of the respective phase states of the two phospholipids at 20°C and showed  
47  
48  
49 97 that AFM indentation is a sensitive method to assess the mechanical properties of 3D  
50  
51  
52 98 membrane objects at the nanoscale.  
53  
54  
55 99

## 100 II. EXPERIMENTAL METHODS

## 101 **2.1. Materials**

102 Pure phospholipids 1,2-dioleoyl-sn-glycero-3-phosphocholine (DOPC; 18:1; >99%) and 1,2-  
103 dipalmitoyl-sn-glycero-3-phospholcholine (DPPC; 16:0; >99%) were purchased from Avanti  
104 Polar Lipids (Alabaster, AL). PIPES (1,4-piperazinediethanesulfonic acid) buffer was  
105 prepared as: PIPES 10 mM (purity  $\geq$ 99%; Sigma-Aldrich, Milwaukee, WI, USA), NaCl 50  
106 mM (Sigma), and CaCl<sub>2</sub> 10 mM (Sigma) were dissolved in Milli-Q water and adjusted to pH  
107 6.7 using NaOH 5 M.

## 108 **2.2. Preparation of liposomes**

109 Samples were prepared by dissolving appropriate quantity of the lipid powder of DOPC or  
110 DPPC in glass vials with chloroform/methanol (4:1 v/v). The organic solvent was then  
111 evaporated at 40 °C under a stream of dry nitrogen. The dried lipid films were hydrated with  
112 PIPES-NaCl-CaCl<sub>2</sub> buffer at 70°C to reach a final concentration of 0.1 wt. % lipids then  
113 thoroughly vortexed. Small unilamellar vesicles (SUV) were produced at 65°C by sonication  
114 using a Q700 equipment (Q-sonica, Newtown, CT, USA) and a microtip operating at 50%  
115 amplitude (~400 W) for 30 min. After sonication, the SUV suspension was left to cool and  
116 equilibrate at room temperature (20°C). The SUV produced according to this protocol will be  
117 designated as “liposomes” throughout this report.

## 118 **2.3. Dynamic light scattering (DLS)**

119 The size distribution and the average hydrodynamic diameter ( $D_h$ ) of the vesicles were  
120 measured in PIPES-NaCl-CaCl<sub>2</sub> buffer at 20°C by dynamic light scattering (DLS) on a

1  
2  
3 121 Zetasizer Nano ZS (Malvern Instruments, Worcestershire, United Kingdom). Measurements  
4  
5 122 were carried out at a scattering angle of  $173^\circ$  and a wavelength of 633 nm. The average  $D_h$  ( $\pm$   
6  
7  
8 123 5 nm) was calculated from the intensity distribution using conversion into an autocorrelation  
9  
10  
11 124 function which is then analyzed with the Stokes-Einstein relation, assuming that particles had  
12  
13  
14 125 a spherical shape. The viscosity of the solution was 1.003 mPa.s at  $20^\circ\text{C}$  and the refractive  
15  
16  
17 126 index of the solvent was 1.33.

#### 127 **2.4. Differential scanning calorimetry (DSC)**

128 The thermotropic properties of DOPC or DPPC were measured on multilamellar vesicles  
129 using a differential scanning calorimetry (DSC) Q1000 apparatus (TA Instruments,  
130 Newcastle, USA). Multilamellar vesicles (MLV) were produced by rehydration of the lipid  
131 films with PIPES-NaCl-CaCl<sub>2</sub> buffer at  $65^\circ\text{C}$  to reach a final concentration of 20 wt. % lipids,  
132 then thorough vortex mixing. MLV are preferred over unilamellar vesicles in order to  
133 accommodate the high bilayer concentration. They also allow higher resolution of the DSC  
134 thermograms thanks to higher cooperativity of the molecules<sup>30</sup>. The samples were introduced  
135 in 20  $\mu\text{L}$  aluminum pans that were then hermetically sealed. An empty pan was used as a  
136 reference. The samples were heated at  $2^\circ\text{C}\cdot\text{min}^{-1}$  from  $-40^\circ\text{C}$  to  $70^\circ\text{C}$ . The calibration of the  
137 calorimeter was performed with indium standard (melting point =  $156.66^\circ\text{C}$ ,  $\Delta H$  melting =  
138  $28.41 \text{ J}\cdot\text{g}^{-1}$ ). The thermal measurements were performed in triplicate. Standard parameters  
139 were calculated by the TA software (Universal Analysis 2000, v 4.1 D).

#### 140 **2.5. Temperature-controlled X-ray diffraction (XRD)**



1  
2  
3 141 X-ray scattering experiments were performed on the home-made Guinier beamline at IPR<sup>31</sup> .  
4  
5 142 A two-dimensional Pilatus detector with sample to detector distance of 232 mm allowed the  
6  
7  
8 143 recording of XRD patterns in the range 0.013 Å<sup>-1</sup> to 1.742 Å<sup>-1</sup>, thus covering both the small  
9  
10  
11 144 and wide-angles regions of interest to characterize the lamellar structures and to identify the  
12  
13  
14 145 packing of the acyl chains, respectively. Diffraction patterns displayed series of concentric  
15  
16  
17 146 rings as a function of the radial scattering vector  $q = 4 \pi \sin\theta / \lambda$ , where  $2\theta$  is the scattering  
18  
19  
20 147 angle and  $\lambda = 1.541 \text{ \AA}$  is the wavelength of the incident beam. The channel to scattering vector  
21  
22  
23 148  $q$  calibration of the detector was carried out with silver behenate<sup>32</sup>. Small volumes (around 10  
24  
25 149  $\mu\text{L}$ ) of samples containing DOPC or DPPC vesicles were loaded in thin quartz capillaries of  
26  
27  
28 150 1.5 mm diameter (GLAS W. Muller, Berlin, Germany) and inserted in the set-up at a  
29  
30  
31 151 controlled temperature.

## 32 33 152 **2.6. Transmission electron microscopy (TEM)**

34  
35  
36 153 The observation of DOPC and DPPC Liposomes by cryo-TEM was realized as described in  
37  
38  
39 154 previous work<sup>33</sup>. The samples were prepared using a cryoplunge cryo-fixation device (Gatan,  
40  
41  
42 155 Pleasanton, CA, USA) in which a drop of the aqueous suspension was deposited on to glow-  
43  
44  
45 156 discharged holey-type carbon-coated grids (Ted Pella Inc., Redding, CA, USA). The TEM  
46  
47  
48 157 grid was then prepared by blotting the drop containing the specimen to a thin liquid layer  
49  
50  
51 158 remained across the holes in the support carbon film. The liquid film was vitrified by rapidly  
52  
53  
54 159 plunging the grid into liquid ethane cooled by liquid nitrogen. The vitrified suspension of  
55  
56 160 liposomes was mounted in a Gatan 910 specimen holder that was inserted in the microscope  
57  
58  
59  
60

1  
2  
3 161 using a CT-3500-cryotransfer system (Gatan, USA) and cooled with liquid nitrogen. TEM  
4  
5 162 images were then obtained from liposomes suspension preserved in vitreous ice and  
6  
7  
8 163 suspended across a hole in the supporting carbon substrate. The samples were observed under  
9  
10  
11 164 low dose conditions ( $< 10 \text{ e}^-/\text{Å}^2$ ), at  $-178 \text{ °C}$ , using a JEM 1230 'Cryo' microscope (Jeol,  
12  
13  
14 165 Japan) operated at 80 keV and equipped with a LaB6 filament. All the micrographs were  
15  
16  
17 166 recorded on a Gatan 1,35 K  $\times$  1,04 K  $\times$  12 bit ES500W CCD camera.

## 18 19 20 167 **2.7. Atomic force microscopy (AFM)**

### 21 22 168 **2.7.1. Indentation of liposomes**

23  
24  
25 169 Simple open liquid sample cells were fabricated by gluing small ( $\sim 0.5 \times 1 \text{ cm}^2$ ) pieces of  
26  
27  
28 170 silicon substrate (molecular orientation 100) onto diagnostic glass slides (Thermo Scientific,  
29  
30  
31 171 Waltham, MA, USA). After thorough cleaning of the cell with ethanol, water and UV/O<sub>3</sub>, the  
32  
33  
34 172 liposome suspension equilibrated at 20°C was deposited onto the clean silicon surface then  
35  
36  
37 173 left to incubate at 20°C for 30 min. The droplet was then gently exchanged with PIPES-NaCl-  
38  
39  
40 174 CaCl<sub>2</sub> buffer at 20°C to remove the un-adsorbed liposomes. The sample was then imaged in  
41  
42  
43 175 contact mode using an MFP-3D Bio AFM (Asylum Research, Santa Barbara, CA, USA), with  
44  
45  
46 176 a typical scan rate of 1 Hz for  $20 \times 20 \text{ }\mu\text{m}^2$  and  $256 \times 256$  pixels images, silicon MLCT  
47  
48  
49 177 probes (nominal spring constant  $k \sim 0.03 \text{ N.m}^{-1}$  – Bruker Nano Surfaces, Santa Barbara, CA,  
50  
51  
52 178 USA) calibrated extemporaneously using the thermal noise method, and loading forces  
53  
54  
55 179 typically below 1 nN. Upon adsorption onto the flat surface, the spherical liposomes deform  
56  
57  
58 180 into spherical cap geometry. AFM imaging of large area (typical size) allows localization of  
59  
60

1  
2  
3 181 the adsorbed liposomes, then closer images (typically  $2 \times 2 \mu\text{m}^2$  or less) were recorded and  
4  
5  
6 182 sections were drawn across the images in order to measure the individual liposome's height  
7  
8  
9 183 (H) and base width (W). The AFM probe was then positioned above the center of each  
10  
11 184 liposome and individual force curves ( $n > 60$ ) were recorded with a set point of 200 pN, a  
12  
13  
14 185 distance of 100 nm and a Z-piezo speed of  $2 \mu\text{m}\cdot\text{s}^{-1}$ . In these conditions, indentation of the  
15  
16  
17 186 AFM tip into the liposome did not exceed  $\sim 5$  nm, thereby allowing measurement of the  
18  
19  
20 187 mechanical properties in the elastic regime of the membrane. The approach curves were then  
21  
22 188 treated using the shell theory as described in the result section.

23  
24  
25 189 For data visualization and analysis, Gwyddion 2.47 software was also used, as a means to  
26  
27  
28 190 deduce the local radius of curvature ( $R_c$ ) at the top of individual adsorbed liposomes over a  
29  
30  
31 191 distance of  $\sim 130$  nm both sides of the apex (130 nm being the estimated radius of the  
32  
33  
34 192 membrane area affected by indentation by a 20-nm radius MLCT probe). The  $R_c$  values of  
35  
36  
37 193 individual liposomes were input in the calculation of the Young modulus (see below).  
38  
39 194 Measurement of the local  $R_c$  values at the apex of individual liposomes, instead of for the  
40  
41  
42 195 complete objects, avoided errors due to imperfect (e.g. flattened) spherical cap geometry of  
43  
44  
45 196 the liposome upon adsorption, and/or errors due to convolution by the AFM tip. The latter  
46  
47  
48 197 may indeed overestimate lateral dimensions of the liposomes by as much as the tip diameter,  
49  
50  
51 198 but can be avoided as long as near-normal contact is maintained between the tip and the  
52  
53 199 liposomes, which is the case when measuring  $R_c$  at their apex.

### 200 **2.7.2. Measurement of the bilayer thickness**

1  
2  
3 201 Immediately after sonication at 65°C, 10 µg of the hot lipid suspension were deposited onto  
4  
5  
6 202 freshly cleaved mica in an Asylum Research open liquid cell, then incubated at 65°C for 60  
7  
8  
9 203 min. Slow cooling of the samples was performed using a programmed incubator as in Murthy  
10  
11 204 et al.<sup>34</sup> to yield supported lipid bilayers (SLB). Once equilibrated at 20°C, the bilayers were  
12  
13  
14 205 extensively rinsed and exchanged with PIPES-NaCl-CaCl<sub>2</sub> buffer. AFM imaging of the  
15  
16  
17 206 bilayers was then performed in the same buffer and in contact mode using MSNL probe  
18  
19  
20 207 (nominal spring constant  $k \sim 0.03 \text{ N.m}^{-1}$  – Bruker Nano Surfaces, Santa Barbara, CA, USA)  
21  
22  
23 208 with the same imaging parameters already cited. The probes were calibrated  
24  
25  
26 209 extemporaneously using the thermal noise method. Force spectroscopy curves were then  
27  
28  
29 210 acquired at 20°C by using force-volume imaging of the bilayers (typically  $10 \times 10 \text{ µm}^2$  or  
30  
31 211 less) with a typical set point of 20 nN and a piezo speed of  $2 \text{ µm.s}^{-1}$ .

## 33 212 **2.8. Statistical analysis**

34  
35  
36 213 The results are presented as mean value  $\pm$  standard deviation. Analysis of variance was  
37  
38  
39 214 performed using the General Linear Model procedure of Statgraphics Plus version 5  
40  
41  
42 215 (Statistical Graphics Corp., Englewood Cliffs, NJ). Differences were significant for  $p < 0.05$ .

43  
44  
45 216

## 47 217 **III. RESULTS AND DISCUSSION**

### 50 218 **3.1. Phase state of DOPC and DPPC at 20°C**

51  
52  
53 219 The thermal phase behavior of unsaturated (18:1) DOPC and saturated (16:0) DPPC  
54  
55  
56 220 phospholipids (chemical structures shown in Fig1.A) was examined using DSC and the  
57  
58  
59  
60

1  
2  
3 221 results were correlated with the structural analysis performed by XRD. Fig1.B shows the  
4  
5  
6 222 respective DSC heating thermograms of both lipids in the same conditions. For DOPC, the  
7  
8  
9 223 thermogram shows a very low temperature of  $L_{\beta}$  to  $L_{\alpha}$  (gel to fluid) phase transition at  $T_m = -$   
10  
11 224  $20^{\circ}\text{C}$ , in good agreement with previous reports <sup>11,35,36</sup>. Meanwhile, the heating of DPPC  
12  
13  
14 225 revealed two endotherms, characteristic of the  $L_{\beta}$  (gel) to  $P_{\beta}$  (ripple) transition at  
15  
16  
17 226  $T_m = 37.09^{\circ}\text{C}$  and of the  $P_{\beta}$  (ripple) to  $L_{\alpha}$  (fluid) transition at  $T_m = 41.01^{\circ}\text{C}$ , also in good  
18  
19  
20 227 agreement with previous reports <sup>34,35,37</sup>. XRD experiments allowed identification of the lipid  
21  
22 228 phases at  $20^{\circ}\text{C}$  (Fig. 1C). For this, the MLV are interesting not only to investigate the lateral  
23  
24  
25 229 packing of the acyl chains (at large  $q$ ), but also to confirm the lamellar organization of the  
26  
27  
28 230 phospholipid (at small  $q$ ). For DOPC, the absence of diffraction peak at wide angles and a  
29  
30  
31 231 lamellar organization characterized at small angles, confirmed the  $L_{\alpha}$  phase of DOPC at  $20^{\circ}\text{C}$ .  
32  
33  
34 232 DPPC multilamellar vesicles exhibited a single broad peak at  $q \sim 1.5 \text{ \AA}^{-1}$  corresponding to the  
35  
36  
37 233 formation of ordered phase packed in pseudo-hexagonal lattice and a lamellar organization at  
38  
39  
40 234 small angles, showing the formation of a  $L_{\beta}$  organization of DPPC at  $20^{\circ}\text{C}$ . The tilt of the  
41  
42  
43 235 acyl chains may have been induced by the multilamellar organization of the DPPC molecules  
44  
45  
46 236 in the vesicles. Since AFM experiments on DPPC molecules were performed in SUV, the  
47  
48  
49 237 ordered phase state of DPPC molecules in SUV at  $20^{\circ}\text{C}$  was also proved by XRD  
50  
51 238 experiments performed on SUV of DPPC. As previously reported in literature<sup>38</sup>, the high  
52  
53  
54 239 curvature of expected SUV of DPPC do not allow the recording of a peak at wide angles.  
55  
56  
57 240 Nevertheless, the Small Angles X-ray Scattering could be performed upon heating of the  
58  
59  
60

1  
2  
3 241 SUV. Both high and low temperature spectra can be fitted as an individual membrane using  
4  
5 242 equation (1):  
6  
7

8 243  
9

10  
11  
12 244 
$$I(q) = \frac{1}{q^2} \left[ \frac{\sin(q.e_{HG}/2)}{q.e_{HG}} . e^{-(q.r)^2} + \frac{\sin(q.e_{CH2}/2)}{q.e_{CH2}} \right]^2 \quad (1)$$
  
13  
14

15  
16 245 with  $e_{HG}$ , the headgroup thickness,  $e_{CH2}$ , the aliphatic chain thickness and  $r$  the rugosity of the  
17  
18 246 headgroup/water interface.  
19

20  
21  
22 247 The full analysis demonstrates a contraction of 2Å of both  $e_{HG}$  and  $e_{CH2}$  at the gel-fluid  
23  
24 248 transition at 40-44°C (Fig. 1D). This showed that the DPPC molecules in SUV are sensitive to  
25  
26 249 temperature and consequently in the gel phase at room temperature. In conclusion, DSC and  
27  
28 250 XRD confirmed that DOPC (unsaturated;  $T_m = -20^\circ\text{C}$ ) and DPPC (saturated;  $T_m = 41^\circ\text{C}$ )  
29  
30 251 were respectively present in fluid and gel phases at 20°C.  
31  
32

### 33 252 **3.2. Morphology of the liposomes at 20°C**

34  
35

36 253 Electron microscopy, dynamic light scattering (DLS) and AFM imaging were used to  
37  
38 254 characterize the morphology (size and shape) of the liposomes obtained after sonication (Fig  
39  
40 255 2). Cryo-TEM images showed that DOPC and DPPC vesicles were essentially unilamellar  
41  
42 256 and spherically shaped. However, while DOPC liposomes consistently exhibited circular  
43  
44 257 cross-sections (Fig 2A), DPPC could show both rounded and/or somewhat faceted  
45  
46 258 membranes (Fig 2D). The presence of angle facets was attributed to the physical gel state of  
47  
48 259 DPPC at 20°C<sup>39</sup>. Cryo-TEM images revealed variable liposome diameters (from tens to  
49  
50  
51  
52  
53  
54  
55  
56  
57  
58  
59  
60

1  
2  
3 260 hundreds of nm) which corresponded to the size distribution measured by DLS (Fig 2B, E).

4  
5 261 For DOPC, the size distribution was monomodal with a mean diameter  $D_h$  at  $120 \pm 69$  nm

6  
7  
8 262 (Fig 2.B). Whereas, DPPC liposomes exhibited a shouldered size distribution with a mean

9  
10 263 diameter  $D_h$  of  $132 \pm 73$  nm for the whole distribution (Fig 2.E; Table1).

11  
12  
13  
14 264 In the next step, the liposomes were immobilized by adsorption onto silicon to be first

15  
16  
17 265 imaged then indented using an AFM probe. Images recorded in contact mode showed that

18  
19  
20 266 DOPC and DPPC liposomes were perfectly stable on the flat substrate. However, it was

21  
22  
23 267 not possible to prevent non-destructive deformation due to adsorption, as previously

24  
25 268 reported<sup>19,40</sup>. The AFM images were also used to measure the height  $H$  and basal width  $W$

26  
27  
28 269 of adsorbed individual liposomes in order to prove that objects observed in AFM images

29  
30  
31 270 corresponded truly to liposomes. To do this, the adsorbed liposomes were considered to

32  
33  
34 271 adopt a spherical cap geometry and their volume was calculated as:

35  
36  
37  
38  
39  
40  
41  
42  
43  
44  
45  
46  
47  
48  
49  
50  
51  
52  
53  
54  
55  
56  
57  
58  
59  
60

$$V = \frac{\pi H}{6} \left( \frac{3}{4} W^2 + H^2 \right) \quad (2)$$

272 From (Eq.2), the mean diameter of a sphere of equivalent volume was inferred and compared

273 with DLS data (Table 1; Figures 2B and E). The mean diameter values were of similar orders

274 of magnitude in both methods; and whatever the method used, DOPC liposomes always

275 exhibited smaller diameters than DPPC ones. This confirmed that the adsorbed objects visible

276 on the AFM images truly were liposomes. However, the mean diameter results measured by

277 AFM were higher than DLS probably because larger liposomes were preferably chosen out of

1  
2  
3 278 large-area images (such as shown on Figure 2) to perform close-up views and indentation  
4  
5 279 measurements (Table1).  
6  
7

### 8 280 **3.3. Mechanical properties of liposomes as a function of phase state at 20°C**

#### 9 281 **3.3.1. Bilayer thickness**

10  
11  
12 282 The average bilayer thickness  $d$  was measured in the conditions used in this work:  
13  
14 283 temperature 20°C, pH=6.7, 50 mM NaCl and 10 mM CaCl<sub>2</sub>. This measurement was  
15  
16  
17 284 performed using atomic force spectroscopy on SLB of DOPC or DPPC spread onto freshly  
18  
19  
20 285 cleaved mica. Average values of  $d$  were obtained from measurements performed on various  
21  
22  
23 286 regions of different samples ( $n=50$ ). In a typical force spectroscopy experiment, the AFM tip  
24  
25  
26 287 approaches the surface until a mechanical contact with the SLB is established. Then, the  
27  
28  
29 288 bilayer is elastically deformed by the AFM probe until the tip ruptures (breaks through) the  
30  
31  
32 289 membrane, thereby coming into contact with the substrate. The indentation *vs* force curves  
33  
34  
35 290 exhibited breakthrough events<sup>23,34,41</sup> where the jump-through distance (noted  $d$ ) was  
36  
37  
38 291 assimilated as the bilayer's thickness<sup>34</sup>. The limitations of this measurement were discussed  
39  
40  
41 292 elsewhere<sup>42</sup> and efforts were taken to regard bilayer compression. Fig.3A and C show three  
42  
43  
44 293 examples of force-distance curves for each type of lipid bilayer. The  $d$  mean values obtained  
45  
46  
47 294 were  $3.91 \pm 0.46$  nm, and  $4.93 \pm 0.47$  nm for DOPC and DPPC bilayers, respectively. This  
48  
49  
50 295 thickness difference between fluid and gel phases was perfectly detected by AFM  
51  
52  
53 296 spectroscopy, in agreement with previous works<sup>25,43</sup>. In the literature, Nagles and Tristram-  
54  
55  
56 297 Nagles<sup>44</sup> also determined the thicknesses of DOPC and DPPC fully hydrated bilayers using  
57  
58  
59  
60



1  
2  
3 298 XRD and obtained a value of 3.6 nm for DOPC in the fluid phase and of 4.4 nm for DPPC in  
4  
5  
6 299 the gel phase. It should be noted that DOPC has two unsaturated 18 hydrocarbon chains and  
7  
8  
9 300 DPPC has two fully saturated 16 hydrocarbon chains (Fig1A). Unsaturation is the main  
10  
11 301 reason that adversely affected chain elongation and molecular packing<sup>45</sup>, making DPPC  
12  
13  
14 302 bilayers more ordered and thicker than DOPC bilayers at room temperature.  
15  
16  
17 303 Noteworthy, the value of the force at which the SLB ruptured (i.e., the breakthrough force)  
18  
19 304 was higher for DPPC (2-3 nN) than for DOPC (<1 nN), in agreement with their respective  
20  
21  
22 305 phase states<sup>46-48</sup>. The lower absolute values found in the present study may be accounted for  
23  
24  
25 306 the lower ionic strength and the sharper AFM tip (radius of MNSL tip ~2 nm) in comparison  
26  
27  
28 307 to previous works.

### 308 **3.3.2. Mechanical properties of DOPC or DPPC liposomes:**

309 In this work, we show that AFM spectroscopy could be used to discriminate and compare the  
310  
311 mechanical properties of very small liposomes (~150 nm) in different phase states.  
312  
313 Calculations of the Young modulus  $E$  and bending modulus  $k_C$ , based on the shell theory  
314  
315 model, were done on DOPC or DPPC liposomes respectively in fluid or gel phase. In order to  
316  
317 limit the plastic deformation, force distance curves were recorded over 100 nm distance with a  
318  
319 set point of 200 pN maximal force. Typical examples are shown in Fig. 3 B and D. In these  
320  
321 conditions, the approaching and retracting curves were superimposed, demonstrating the  
322  
323 elastic behavior of the membrane (not shown). The tip-membrane contact was defined as the  
324  
325 point where significant positive slope appeared. According to the shell theory developed by

1  
2  
3 318 Reissner<sup>49</sup> then Fery et al.<sup>16,50</sup>, the Young modulus  $E$  of thin-shelled spherical micro-capsule  
4  
5  
6 319 under a point load scales with the bilayer's stiffness,  $k$ , which was deduced from the slope of  
7  
8  
9 320 the linear region of each force curve after the tip-membrane contact, i.e. in the small  
10  
11 321 deformation region (Fig 3.B and D). As  $k$  strongly depends on the size of the individual  
12  
13 322 liposomes<sup>21</sup>, it has to be normalized by the local radius of curvature  $R_c$  of the individual  
14  
15 323 liposomes<sup>16</sup> to describe their mechanical properties. Calculation of  $E$  requires the bilayers'  
16  
17 324 stiffness  $k$ , the local radius of curvature  $R_c$  (see section 2.7.1), the bilayer's thickness  $d$   
18  
19  
20  
21  
22 325 (Table1) and the Poisson ratio  $\nu$ , taken as 0.5:

$$E = \frac{1}{C} \frac{kR_c \sqrt{3(1-\nu^2)}}{4d^2} \quad (3)$$

23  
24  
25  
26  
27  
28  
29 326 In equation 3,  $C$  is a coefficient that accounts for the double deformation of an adsorbed shell  
30  
31 327 object, such as liposomes, upon indentation by the AFM tip. Indeed, whereas membrane  
32  
33 328 deformation occurs at the contact point between the tip and the liposome, simultaneous  
34  
35 329 deformation also occurs at the contact area between the liposome and the substrate<sup>51</sup>. In their  
36  
37  
38  
39 330 recent paper, Bery et al.<sup>52</sup> produced calculations for a correction factor,  $C$ , to be applied as a  
40  
41 331 function of the relative radii of the tip (20 nm) and liposome, and of the shell thickness  
42  
43 332 relative to the radius of the liposomes (Table 1). Since that dimensions were similar for both  
44  
45 333 the DOPC and DPPC liposomes,  $C$  was  $\sim 0.55$  for both types of liposomes.

46  
47  
48  
49 334 In another way, the mechanical properties of liposomes can be also represented by the  
50  
51 335 bending rigidity  $k_C$ , which is expressed in terms of the same parameters and is also common in  
52  
53  
54  
55 336 the literature:

$$k_C = \frac{Ed^3}{12(1-\nu^2)} \quad (4)$$

1  
2  
3  
4  
5  
6  
7  
8  
9  
10  
11  
12  
13  
14  
15  
16  
17  
18  
19  
20  
21  
22  
23  
24  
25  
26  
27  
28  
29  
30  
31  
32  
33  
34  
35  
36  
37  
38  
39  
40  
41  
42  
43  
44  
45  
46  
47  
48  
49  
50  
51  
52  
53  
54  
55  
56  
57  
58  
59  
60

337 Calculation of the Young's modulus, regardless of liposome size, showed that the DPPC  
338 liposome membranes ( $L_\beta$ )  $E= 116 \pm 45$  MPa were significantly more elastic at 20°C than  
339 DOPC liposome membranes ( $L_\alpha$ ) which exhibited a lower value of  $E = 13 \pm 9$  MPa (Fig.4.A  
340 and B;  $p < 0.05$ ). Accordingly, the liposome membranes composed of DPPC were also stiffer  
341 with  $k_C = (15.5 \pm 6) \times 10^{-19}$ J (360  $k_B$ T) than those composed of DOPC with  $k_C = (0.9 \pm 0.6)$   
342  $\times 10^{-19}$ J (22  $k_B$ T) (Fig.4.C and D;  $p < 0.05$  ). To verify that electrostatic repulsion was not  
343 implicated in the force curves near the contact point, we compared the results acquired on  
344 DPPC liposomes with varying surface charge, taken as the zeta potential and measured as  
345 described in Makino et al.<sup>53</sup>. The DPPC liposomes were positively charged with a zeta  
346 potential of 18 mV in PIPES buffer (ionic strength  $I=0.09$ ); and barely charged with a zeta  
347 potential of 0.11 mV in PBS buffer (14 mM  $\text{KH}_2\text{PO}_4$ , 200 mM  $\text{Na}_2\text{HPO}_4$ , NaCl 1.36 M, KCl  
348 20 mM;  $I=1.99$ ;  $\text{pH}= 7.2$ ). The Young's modulus showed a mean value of  $E= 120 \pm 39$  MPa  
349 in PBS buffer and no significant difference was found between the Young moduli values  
350 obtained in the two buffers ( $p > 0.05$ ). This result showed that force measurement of DPPC  
351 membrane was not influenced by electrostatic interaction between the AFM probe and the  
352 liposomes.

353 The Young modulus was also estimated using the  $R_c$  of the whole liposome, which involves  
354 the two parameters  $H$  and  $W$  (equation A.1). The results showed that the elasticity of DPPC

1  
2  
3 355 was higher (183 MPa) than that obtained by local  $R_c$  (116 MPa), whereas  $E$  was not  
4  
5  
6 356 significantly changed for DOPC. With either methods of  $R_c$  calculation, the results therefore  
7  
8  
9 357 showed that AFM indentation was able to detect significant differences in the elasticities of  
10  
11 358 the two membranes depending on their fluid or gel phase state. However, the quantification of  
12  
13  
14 359 the mechanical properties was found very sensitive to calculation of  $R_c$  and to the liposome  
15  
16  
17 360 geometry. For these reasons, we chose to compare the liposomes using the method based on  
18  
19  
20 361 the local  $R_c$  using Gwyddion in order to avoid any effect due to the form adopted by the  
21  
22 362 liposomes upon adsorption.

23  
24  
25 363 In conclusion, the structural differences between the fluid-phase DOPC and gel-phase DPPC  
26  
27  
28 364 bilayers as evidenced by DSC and XRD, induced by the unsaturation of the acyl chains  
29  
30  
31 365 (Fig1), resulted in significant difference in their respective mechanical responses. Hence,  
32  
33 366 AFM force spectroscopy proved a sensitive method to compare the mechanical properties of  
34  
35  
36 367 small liposomes with different lipid compositions and phase states. Only few reports exist that  
37  
38  
39 368 have evaluated these mechanical parameters for similar systems of lipid membrane in 3D,  
40  
41  
42 369 especially for DOPC or DPPC using AFM spectroscopy (Table 2). Of all these studies, only  
43  
44  
45 370 Liang et al.<sup>21</sup> used AFM spectroscopy comparatively, on liposomes with increasing addition  
46  
47  
48 371 of cholesterol. Liang et al.<sup>21</sup> obtained Young's modulus of  $1.97 \pm 0.75$  MPa, for liposomes in  
49  
50  
51 372 the fluid phase composed of egg PC (mixture of saturated and unsaturated polar lipids; mostly  
52  
53  
54 373 in the form of SOPC – stearyl-oleoyl-phosphatidylcholine). Using an optical method,  
55  
56 374 Meleard et al.<sup>54</sup> and Duwe et al.<sup>55</sup> respectively obtained bending rigidities of  $1.27 \pm 0.09 \times 10^{-7}$

1  
2  
3 375  $^{19}\text{J}$  ( $31 k_{\text{B}}\text{T}$ ) or  $1.15 \times 10^{-19}\text{J}$  ( $28 k_{\text{B}}\text{T}$ ) for liposomes composed of the saturated polar lipid  
4  
5 376 DMPC (1,2-dimyristoyl-sn-glycero-3-phosphocholine) in fluid phase at  $40^{\circ}\text{C}$  ( $T_{\text{m}} = 24^{\circ}\text{C}$ ).  
6  
7  
8 377 Rawicz et al.<sup>45</sup> found values of  $\sim 0.9 \times 10^{-19}$  J for bilayers of various synthetic 18:1  
9  
10  
11 378 phospholipids. Another group, Hantz et al.<sup>56</sup> used the osmotic swelling method and found  
12  
13  
14 379 values of the Young's modulus of 15 MPa for DOPC liposomes in the fluid phase at  $20^{\circ}\text{C}$ .  
15  
16  
17 380 Delorme and Fery<sup>16</sup> obtained Young's moduli values of  $110 \pm 15$  MPa for DPPC liposomes in  
18  
19  
20 381 the gel phase. Taking only account of the phase state conditions, the values available in the  
21  
22 382 literature (Table 2) are in the same order of magnitude in comparison to the results showed in  
23  
24  
25 383 this work. Differences between studies could be attributed mainly to the nature of the lipids  
26  
27  
28 384 (carbon chain length, number of unsaturation), the temperature, the chosen technique or, for  
29  
30  
31 385 indentation studies, the mathematical model chosen for the calculation of  $R_{\text{c}}$  or  $E$ <sup>57,58</sup>. The  
32  
33  
34 386 presented results show that AFM indentation of liposome is a sensible method for comparison  
35  
36  
37 387 between different lipid membranes.  
38  
39  
40 388 For the sake of comparison with the SUV (tridimensional organization), the elasticity of  
41  
42  
43 389 DPPC or DOPC membranes was calculated on the SLB (two dimensional organization) using  
44  
45  
46 390 AFM load curves performed in the same conditions as for the breakthrough force  
47  
48  
49 391 measurement. Only a larger MLCT probe was used for better sensibility. By attempting the  
50  
51  
52 392 fit of equation (5), the Young's moduli (noted  $E_{\text{SLB}}$ ) and bending modulus (noted  $k_{\text{C-SLB}}$ )  
53  
54  
55 393 were calculated using the classical Hertz model:  
56  
57  
58  
59  
60

$$F = \frac{4E_{SLB}\sqrt{R_{tip}}\delta^{\frac{3}{2}}}{3(1-\nu^2)} \text{ or } E_{SLB} = \frac{3k(1-\nu^2)}{4\sqrt{R_{tip}}\delta} \quad (5)$$

394 For which corresponds a bending modulus:

$$k_{C-SLB} = \frac{E_{SLB}\delta^3}{24(1-\nu^2)} \quad (6)$$

395

396 Where the parameters are the same already cited for liposome membranes. In these equations,

397  $\delta$  is the indentation distance and  $R_{tip}$  is the nominal radius of AFM MLCT tip ( $\sim 20$  nm).

398 The use of contact mechanics using the Hertz model on SLB is limited by the effect of

399 confinement of the sample between the tip and the underlying substrate<sup>59,60</sup>. Furthermore,

400 lipid bilayers are not anisotropic materials. However, previous investigations suggested that

401 this calculation yet has comparative interest<sup>25,61</sup>. On SLBs, the Young modulus ( $E$ ) of DOPC

402 was found to be  $27 \pm 8$  MPa with a corresponding bending modulus  $k_C = (0.88 \pm 0.25) \times 10^{-19}$  J,

403 while the  $E$  and  $k_C$  of DPPC were found to be  $31 \pm 12$  MPa and  $(2.03 \pm 0.79) \times 10^{-19}$  J,

404 respectively. Therefore, the  $E$  and  $k_C$  parameters of DPPC and DOPC were less distinct when

405 measured on SLB than on SUV (Table 2). Meanwhile, more dispersed  $E$  values were reported

406 in the literature for SLBs than for liposomes, thereby indicating the higher sensitivity of this

407 measurement upon experimental conditions in the case of SLB<sup>25,61,62</sup> (Table 2). To conclude,

408 it is showed that membranes in the gel phase were more elastic and stiffer than the

409 membranes in fluid phase regardless the lipid organization (2D or 3D). However, the values

410 of  $E$  and  $k_C$  were more robust when measured on liposomes than on SLBs, where the presence

1  
2  
3 411 of the solid support affected the results depending on the indentation distance<sup>25</sup>. These  
4  
5 412 comparisons show that liposomes are adequate systems to determine the elastic properties of  
6  
7  
8 413 lipid membranes. On the other hand, measurement of the breakthrough force is relevant for  
9  
10  
11 414 SLBs.

12  
13  
14 415 The structure of molecules and the intermolecular interactions that lead lipid molecules to  
15  
16 416 self-assembly in bilayers, have a significant impact on the rigidity of these bilayers<sup>63,64</sup>. The  
17  
18 417 elasticity of the membrane allows it to accommodate strain without failure, which is essential  
19  
20 418 in many applications where the membrane need to resist shear stress, e.g. in transdermal  
21  
22 419 application, in blood vessels, the epithelial cells of the gastrointestinal tract, etc. The  
23  
24 420 hydrophobic interactions between the lipid molecules, in particular Van der Vaal interactions,  
25  
26 421 are the major responsible of the fluidity and the rigidity of the membrane. The double bond in  
27  
28 422 cis conformation interferes with hydrocarbon chain packing and destroys the cooperativity of  
29  
30 423 the chain interactions in the bilayer<sup>65,66</sup>.

31  
32  
33 424 The presence of this double bonds reduces the hydrophobic interactions by increasing the  
34  
35 425 distance between the hydrophobic moieties which decreases the stiffness of membrane<sup>45</sup>.

#### 36 426 **IV. CONCLUSION:**

37  
38  
39 427 The nano-indentation of DOPC and DPPC liposomes by AFM probe at low force load was  
40  
41 428 able to provide local and discriminant information on the elastic properties of bilayer  
42  
43 429 membranes in 3D organization without plastic deformation. The Young's moduli  $E$  and  
44  
45 430 bending rigidity values  $k_C$  of gel phase DPPC membranes is significantly higher than that of  
46  
47  
48  
49  
50  
51  
52  
53  
54  
55  
56  
57  
58  
59  
60

1  
2  
3 431 fluid phase DOPC ones at 20°C, in agreement with their different phase state. The  
4  
5  
6 432 perspective of this work is to investigate the mechanical properties of biological membranes  
7  
8  
9 433 with complex chemical composition and fluid/gel phase coexistence. Thanks to the high  
10  
11 434 lateral resolution of AFM, it is expected that phase separation and correlated nanomechanical  
12  
13  
14 435 contrast may be measured directly on model liposomes or even biological vesicles.

## 17 436 **V. ACKNOWLEDGMENTS**

20 437 The Asylum Research MFP3D-BIO atomic force microscope was funded by the European  
21  
22  
23 438 Union (FEDER), the French Ministry of Education and Research, INRA, Conseil Général 35  
24  
25  
26 439 and Rennes Métropole. The doctoral fellowship of author Et-Thakafy was funded by INRA  
27  
28  
29 440 CEPIA and Région Bretagne under the grant ARED 8806.

## 32 441 **VI. APPENDIX:**

35 442 The Young modulus values were also obtained using radius of curvature  $R_C$  of the whole  
36  
37  
38 443 individual liposomes. It was calculated using  $H$  and  $W$  of the individual liposomes<sup>67</sup>  
39  
40  
41 444 , as:

$$44 R_C = \frac{0.25W^2 + H^2}{2H} \quad (A.1)$$

48 445 The mechanical data obtained from literature were expressed either as the Young modulus  $E$ ,  
49  
50  
51 446 the bending rigidity  $k_C$  or both. To complete and compare literature information in table 2; we  
52  
53  
54 447 used the following equations to provide both parameters for each cited reference:

56  
57 448 For liposome (shell model):



$$k_C = \frac{Ed^3}{12(1-\nu^2)} \Rightarrow E = \frac{12(1-\nu^2)k_C}{d^3} = \frac{9k_C}{d^3} \quad (A.2)$$

449 For supported lipid bilayer (Hertz model):

$$k_{C-SLB} = \frac{E_{SLB} d^3}{24(1-\nu^2)} \Rightarrow E_{SLB} = \frac{24(1-\nu^2)k_{C-SLB}}{d^3} = \frac{18k_{C-SLB}}{d^3} \quad (A.3)$$

450  $E$ : Young modulus

451  $k_C$ : bending rigidity

452  $\nu$ : Poisson coefficient (0.5)

453  $d$ : membrane thickness

454 For the publication where the membrane thickness not shown, the following values were used

455 to calculate the elasticity or the bending rigidity:

456  $d(\text{DMPC}) = 3.6 \text{ nm}$  <sup>44</sup>

457  $d(\text{DOPC}) = 3.9 \text{ nm}$  <sup>(present work)</sup>

458

459

## 460 REFERENCES

- 461 (1) Lasic, D. D. Novel Applications of Liposomes. *Trends Biotechnol.* **1998**, *16*, 307–321.
- 462 (2) Liu, W.; Ye, A.; Liu, C.; Liu, W.; Singh, H. Structure and Integrity of Liposomes  
463 Prepared from Milk- or Soybean-Derived Phospholipids during in Vitro Digestion.  
464 *Food Res. Int.* **2012**, *48*, 499–506.
- 465 (3) Théry, C.; Ostrowski, M.; Segura, E. Membrane Vesicles as Conveyors of Immune  
466 Responses. *Nat. Rev. Immunol.* **2009**, *9*, 581–593.
- 467 (4) van der Meel, R.; Fens, M. H.; Vader, P.; van Solinge, W. W.; Eniola-Adefeso, O.;  
468 Schiffelers, R. M. Extracellular Vesicles as Drug Delivery Systems: Lessons from the  
469 Liposome Field. *J. Controlled Release* **2014**, *195*, 72–85.
- 470 (5) Chapman, D. Phase Transitions and Fluidity Characteristics of Lipids and Cell  
471 Membranes. *Q. Rev. Biophys.* **1975**, *8*, 185–235.
- 472 (6) Lipowsky, R. Remodeling of Membrane Compartments: Some Consequences of  
473 Membrane Fluidity. *Biol. Chem.* **2014**, 395.

- 1  
2  
3 474 (7) Neubauer, M. P.; Poehlmann, M.; Fery, A. Microcapsule Mechanics: From Stability to  
4 475 Function. *Adv. Colloid Interface Sci.* **2014**, *207*, 65–80.
- 5 476 (8) Sitterberg, J.; Özçetin, A.; Ehrhardt, C.; Bakowsky, U. Utilising Atomic Force  
6 477 Microscopy for the Characterisation of Nanoscale Drug Delivery Systems. *Eur. J.*  
7 478 *Pharm. Biopharm.* **2010**, *74*, 2–13.
- 8 479 (9) Briuglia, M.-L.; Rotella, C.; McFarlane, A.; Lamprou, D. A. Influence of Cholesterol  
9 480 on Liposome Stability and on in Vitro Drug Release. *Drug Deliv. Transl. Res.* **2015**, *5*,  
10 481 231–242.
- 11 482 (10) Duangjit, S.; Pamornpathomkul, B.; Opanasopit, P.; Rojanarata, T.; Obata, Y.;  
12 483 Takayama, K.; Ngawhirunpat, T. Role of the Charge, Carbon Chain Length, and  
13 484 Content of Surfactant on the Skin Penetration of Meloxicam-Loaded Liposomes. *Int. J.*  
14 485 *Nanomedicine* **2014**, *9*, 2005.
- 15 486 (11) Maherani, B.; Arab-Tehrany, E.; Kheiriloomoom, A.; Cleymand, F.; Linder, M.  
16 487 Influence of Lipid Composition on Physicochemical Properties of Nanoliposomes  
17 488 Encapsulating Natural Dipeptide Antioxidant L-Carnosine. *Food Chem.* **2012**, *134*,  
18 489 632–640.
- 19 490 (12) Tokudome, Y.; Uchida, R.; Yokote, T.; Todo, H.; Hada, N.; Kon, T.; Yasuda, J.;  
20 491 Hayashi, H.; Hashimoto, F.; Sugibayashi, K. Effect of Topically Applied  
21 492 Sphingomyelin-Based Liposomes on the Ceramide Level in a Three-Dimensional  
22 493 Cultured Human Skin Model. *J. Liposome Res.* **2010**, *20*, 49–54.
- 23 494 (13) Yoshimoto, M.; Todaka, Y. Phase Transition-induced Rapid Permeabilization of  
24 495 Liposome Membranes Composed of Milk sphingomyelin. *Eur. J. Lipid Sci. Technol.*  
25 496 **2014**, *116*, 226–231.
- 26 497 (14) Inoue, K. Permeability Properties of Liposomes Prepared from Dipalmitoyllecithin,  
27 498 Dimyristoyllecithin, Egg Lecithin, Rat Liver Lecithin and Beef Brain Sphingomyelin.  
28 499 *Biochim. Biophys. Acta BBA-Biomembr.* **1974**, *339*, 390–402.
- 29 500 (15) Calò, A.; Reguera, D.; Oncins, G.; Persuy, M.-A.; Sanz, G.; Lobasso, S.; Corcelli, A.;  
30 501 Pajot-Augy, E.; Gomila, G. Force Measurements on Natural Membrane Nanovesicles  
31 502 Reveal a Composition-Independent, High Young's Modulus. *Nanoscale* **2014**, *6*, 2275–  
32 503 2285.
- 33 504 (16) Delorme, N.; Fery, A. Direct Method to Study Membrane Rigidity of Small Vesicles  
34 505 Based on Atomic Force Microscope Force Spectroscopy. *Phys. Rev. E* **2006**, *74*.
- 35 506 (17) Laney, D. E.; Garcia, R. A.; Parsons, S. M.; Hansma, H. G. Changes in the Elastic  
36 507 Properties of Cholinergic Synaptic Vesicles as Measured by Atomic Force Microscopy.  
37 508 *Biophys. J.* **1997**, *72*, 806.
- 38 509 (18) Li, S.; Eghiaian, F.; Sieben, C.; Herrmann, A.; Schaap, I. A. Bending and Puncturing  
39 510 the Influenza Lipid Envelope. *Biophys. J.* **2011**, *100*, 637–645.
- 40 511 (19) Liang, X.; Mao, G.; Simon Ng, K. . Probing Small Unilamellar EggPC Vesicles on  
41 512 Mica Surface by Atomic Force Microscopy. *Colloids Surf. B Biointerfaces* **2004**, *34*,  
42 513 41–51.
- 43 514 (20) Ramachandran, S.; Quist, A. P.; Kumar, S.; Lal, R. Cisplatin Nanoliposomes for  
44 515 Cancer Therapy: AFM and Fluorescence Imaging of Cisplatin Encapsulation, Stability,  
45 516 Cellular Uptake, and Toxicity. *Langmuir* **2006**, *22*, 8156–8162.
- 46 517 (21) Liang, X.; Mao, G.; Ng, K. Y. S. Mechanical Properties and Stability Measurement of  
47 518 Cholesterol-Containing Liposome on Mica by Atomic Force Microscopy. *J. Colloid*  
48 519 *Interface Sci.* **2004**, *278*, 53–62.
- 49 520 (22) Benesch, M. G.; McElhaney, R. N. A Comparative Calorimetric Study of the Effects of  
50 521 Cholesterol and the Plant Sterols Campesterol and Brassicasterol on the Thermotropic  
51 522 Phase Behavior of Dipalmitoylphosphatidylcholine Bilayer Membranes. *Biochim.*  
52 523 *Biophys. Acta BBA-Biomembr.* **2014**, *1838*, 1941–1949.

- 1  
2  
3 524 (23) Redondo-Morata, L.; Giannotti, M. I.; Sanz, F. Influence of Cholesterol on the Phase  
4 525 Transition of Lipid Bilayers: A Temperature-Controlled Force Spectroscopy Study.  
5 526 *Langmuir* **2012**, *28*, 12851–12860.
- 6 527 (24) Garcia-Manyes, S.; Sanz, F. Nanomechanics of Lipid Bilayers by Force Spectroscopy  
7 528 with AFM: A Perspective. *Biochim. Biophys. Acta BBA - Biomembr.* **2010**, *1798*, 741–  
8 529 749.
- 9 530 (25) Picas, L.; Rico, F.; Scheuring, S. Direct Measurement of the Mechanical Properties of  
10 531 Lipid Phases in Supported Bilayers. *Biophys. J.* **2012**, *102*, L01–L03.
- 11 532 (26) Ahmed, S.; Nikolov, Z.; Wunder, S. L. Effect of Curvature on Nanoparticle Supported  
12 533 Lipid Bilayers Investigated by Raman Spectroscopy. *J. Phys. Chem. B* **2011**, *115*,  
13 534 13181–13190.
- 14 535 (27) Marbella, L. E.; Yin, B.; Spence, M. M. Investigating the Order Parameters of  
15 536 Saturated Lipid Molecules under Various Curvature Conditions on Spherical Supported  
16 537 Lipid Bilayers. *J. Phys. Chem. B* **2015**, *119*, 4194–4202.
- 17 538 (28) Sorkin, R.; Dror, Y.; Kampf, N.; Klein, J. Mechanical Stability and Lubrication by  
18 539 Phosphatidylcholine Boundary Layers in the Vesicular and in the Extended Lamellar  
19 540 Phases. *Langmuir* **2014**, *30*, 5005–5014.
- 20 541 (29) Buchner Santos, E.; Morris, J. K.; Glynos, E.; Sboros, V.; Koutsos, V. Nanomechanical  
21 542 Properties of Phospholipid Microbubbles. *Langmuir* **2012**, *28*, 5753–5760.
- 22 543 (30) Prenner, E.; Chiu, M. Differential Scanning Calorimetry: An Invaluable Tool for a  
23 544 Detailed Thermodynamic Characterization of Macromolecules and Their Interactions.  
24 545 *J. Pharm. Bioallied Sci.* **2011**, *3*, 39.
- 25 546 (31) Bizien, T.; Ameline, J.-C.; Yager, K. G.; Marchi, V.; Artzner, F. Self-Organization of  
26 547 Quantum Rods Induced by Lipid Membrane Corrugations. *Langmuir* **2015**, *31*, 12148–  
27 548 12154.
- 28 549 (32) Blanton, T.; Barnes, C.; Leental, M. Preparation of Silver Behenate Coatings to  
29 550 Provide Low-to Mid-Angle Diffraction Calibration. *J. Appl. Crystallogr.* **2000**, *33*,  
30 551 172–173.
- 31 552 (33) Gaillard, C.; Douliez, J.-P. Cryo-TEM and AFM for the Characterization of Vesicle-  
32 553 like Nanoparticle Dispersions and Self-Assembled Supramolecular Fatty-Acid-Based  
33 554 Structures: A Few Examples. *Curr. Microsc. Contrib. Adv. Sci. Technol.* **2012**, *5*, 912–  
34 555 922.
- 35 556 (34) Murthy, A. V. R.; Guyomarc'h, F.; Lopez, C. Cholesterol Decreases the Size and the  
36 557 Mechanical Resistance to Rupture of Sphingomyelin Rich Domains, in Lipid Bilayers  
37 558 Studied as a Model of the Milk Fat Globule Membrane. *Langmuir* **2016**, *32*, 6757–  
38 559 6765.
- 39 560 (35) Fa, N.; Ronkart, S.; Schanck, A.; Deleu, M.; Gaigneaux, A.; Goormaghtigh, E.;  
40 561 Mingeot-Leclercq, M.-P. Effect of the Antibiotic Azithromycin on Thermotropic  
41 562 Behavior of DOPC or DPPC Bilayers. *Chem. Phys. Lipids* **2006**, *144*, 108–116.
- 42 563 (36) Fritzsche, K. J.; Kim, J.; Holland, G. P. Probing Lipid–cholesterol Interactions in  
43 564 DOPC/eSM/Chol and DOPC/DPPC/Chol Model Lipid Rafts with DSC and <sup>13</sup>C Solid-  
44 565 State NMR. *Biochim. Biophys. Acta BBA - Biomembr.* **2013**, *1828*, 1889–1898.
- 45 566 (37) Grabielle-Madelmont, C.; Perron, R. Calorimetric Studies on Phospholipid–water  
46 567 Systems: I. Di-Dipalmitoylphosphatidylcholine (DPPC)—water System. *J. Colloid*  
47 568 *Interface Sci.* **1983**, *95*, 471–482.
- 48 569 (38) Boni, L. T.; Minchey, S. R.; Perkins, W. R.; Ahl, P. L.; Slater, J. L.; Tate, M. W.;  
49 570 Gruner, S. M.; Janoff, A. S. Curvature Dependent Induction of the Interdigitated Gel  
50 571 Phase in DPPC Vesicles. *Biochim. Biophys. Acta BBA-Biomembr.* **1993**, *1146*, 247–  
51 572 257.

- 1  
2  
3 573 (39) Kuntsche, J.; Horst, J. C.; Bunjes, H. Cryogenic Transmission Electron Microscopy  
4 574 (Cryo-TEM) for Studying the Morphology of Colloidal Drug Delivery Systems. *Int. J.*  
5 575 *Pharm.* **2011**, *417*, 120–137.
- 6 576 (40) Colas, J.-C.; Shi, W.; Rao, V. M.; Omri, A.; Mozafari, M. R.; Singh, H. Microscopical  
7 577 Investigations of Nisin-Loaded Nanoliposomes Prepared by Mozafari Method and  
8 578 Their Bacterial Targeting. *Micron* **2007**, *38*, 841–847.
- 9 579 (41) Guyomarc'h, F.; Zou, S.; Chen, M.; Milhiet, P.-E.; Godefroy, C.; Vié, V.; Lopez, C.  
10 580 Milk Sphingomyelin Domains in Biomimetic Membranes and the Role of Cholesterol:  
11 581 Morphology and Nanomechanical Properties Investigated Using AFM and Force  
12 582 Spectroscopy. *Langmuir* **2014**, *30*, 6516–6524.
- 13 583 (42) Murthy, A. V. R.; Guyomarc'h, F.; Lopez, C. The Temperature-Dependent Physical  
14 584 State of Polar Lipids and Their Miscibility Impact the Topography and Mechanical  
15 585 Properties of Bilayer Models of the Milk Fat Globule Membrane. *Biochim. Biophys.*  
16 586 *Acta BBA - Biomembr.* **2016**, *1858*, 2181–2190.
- 17 587 (43) Leonenko, Z. V.; Finot, E.; Ma, H.; Dahms, T. E. S.; Cramb, D. T. Investigation of  
18 588 Temperature-Induced Phase Transitions in DOPC and DPPC Phospholipid Bilayers  
19 589 Using Temperature-Controlled Scanning Force Microscopy. *Biophys. J.* **2004**, *86*,  
20 590 3783–3793.
- 21 591 (44) Nagle, J. F.; Tristram-Nagle, S. Structure of Lipid Bilayers. *Biochim. Biophys. Acta*  
22 592 *BBA-Rev. Biomembr.* **2000**, *1469*, 159–195.
- 23 593 (45) Rawicz, W.; Olbrich, K.; McIntosh, T.; Needham, D.; Evans, E. Effect of Chain Length  
24 594 and Unsaturation on Elasticity of Lipid Bilayers. *Biophys. J.* **2000**, *79*, 328–339.
- 25 595 (46) Garcia-Manyes, S.; Oncins, G.; Sanz, F. Effect of Temperature on the Nanomechanics  
26 596 of Lipid Bilayers Studied by Force Spectroscopy. *Biophys. J.* **2005**, *89*, 4261–4274.
- 27 597 (47) Redondo-Morata, L.; Oncins, G.; Sanz, F. Force Spectroscopy Reveals the Effect of  
28 598 Different Ions in the Nanomechanical Behavior of Phospholipid Model Membranes:  
29 599 The Case of Potassium Cation. *Biophys. J.* **2012**, *102*, 66–74.
- 30 600 (48) Jacquot, A.; Francius, G.; Razafitianamaharavo, A.; Dehghani, F.; Tamayol, A.; Linder,  
31 601 M.; Arab-Tehrany, E. Morphological and Physical Analysis of Natural Phospholipids-  
32 602 Based Biomembranes. *PLoS ONE* **2014**, *9*, e107435.
- 33 603 (49) Reissner, E. Note on the Membrane Theory of Shell of Revolution. *Stud. Appl. Math.*  
34 604 **1947**, *26*, 290–293.
- 35 605 (50) Fery, A.; Weinkamer, R. Mechanical Properties of Micro- and Nanocapsules: Single-  
36 606 Capsule Measurements. *Polymer* **2007**, *48*, 7221–7235.
- 37 607 (51) Glaubitz, M.; Medvedev, N.; Pussak, D.; Hartmann, L.; Schmidt, S.; Helm, C. A.;  
38 608 Delcea, M. A Novel Contact Model for AFM Indentation Experiments on Soft  
39 609 Spherical Cell-like Particles. *Soft Matter* **2014**, *10*, 6732.
- 40 610 (52) Berry, J. D.; Mettu, S.; Dagastine, R. R. Precise Measurements of Capsule Mechanical  
41 611 Properties Using Indentation. *Soft Matter* **2017**, *13*, 1943–1947.
- 42 612 (53) Makino, K.; Yamada, T.; Kimura, M.; Oka, T.; Ohshima, H.; Kondo, T. Temperature-  
43 613 and Ionic Strength-Induced Conformational Changes in the Lipid Head Group Region  
44 614 of Liposomes as Suggested by Zeta Potential Data. *Biophys. Chem.* **1991**, *41*, 175–183.
- 45 615 (54) Meleard, P.; Gerbeaud, C.; Pott, T.; Fernandez-Puente, L.; Bivas, I.; Mitov, M. D.;  
46 616 Dufourcq, J.; Bothorel, P. Bending Elasticities of Model Membranes: Influences of  
47 617 Temperature and Sterol Content. *Biophys. J.* **1997**, *72*, 2616.
- 48 618 (55) Duwe, H. de; Sackmann, E. Bending Elasticity and Thermal Excitations of Lipid  
49 619 Bilayer Vesicles: Modulation by Solutes. *Phys. Stat. Mech. Its Appl.* **1990**, *163*, 410–  
50 620 428.
- 51  
52  
53  
54  
55  
56  
57  
58  
59  
60

- 1  
2  
3 621 (56) Hantz, E.; Cao, A.; Escaig, J.; Taillandier, E. The Osmotic Response of Large  
4 622 Unilamellar Vesicles Studied by Quasielastic Light Scattering. *Biochim. Biophys. Acta*  
5 623 *BBA-Biomembr.* **1986**, *862*, 379–386.
- 6 624 (57) Brochu, H.; Vermette, P. Young's Moduli of Surface-Bound Liposomes by Atomic  
7 625 Force Microscopy Force Measurements. *Langmuir* **2008**, *24*, 2009–2014.
- 8 626 (58) Dieluweit, S.; Csiszár, A.; Rubner, W.; Fleischhauer, J.; Houben, S.; Merkel, R.  
9 627 Mechanical Properties of Bare and Protein-Coated Giant Unilamellar Phospholipid  
10 628 Vesicles. A Comparative Study of Micropipet Aspiration and Atomic Force  
11 629 Microscopy. *Langmuir* **2010**, *26*, 11041–11049.
- 12 630 (59) Dimitriadis, E. K.; Horkay, F.; Maresca, J.; Kachar, B.; Chadwick, R. S. Determination  
13 631 of Elastic Moduli of Thin Layers of Soft Material Using the Atomic Force Microscope.  
14 632 *Biophys. J.* **2002**, *82*, 2798–2810.
- 15 633 (60) Shull, K. R. Contact Mechanics and the Adhesion of Soft Solids. *Mater. Sci. Eng. R*  
16 634 *Rep.* **2002**, *36*, 1–45.
- 17 635 (61) Sullan, R. M. A.; Li, J. K.; Zou, S. Direct Correlation of Structures and  
18 636 Nanomechanical Properties of Multicomponent Lipid Bilayers. *Langmuir* **2009**, *25*,  
19 637 7471–7477.
- 20 638 (62) Li, J. K.; Sullan, R. M. A.; Zou, S. Atomic Force Microscopy Force Mapping in the  
21 639 Study of Supported Lipid Bilayers. *Langmuir* **2011**, *27*, 1308–1313.
- 22 640 (63) Marsh, D. Elastic Curvature Constants of Lipid Monolayers and Bilayers. *Chem. Phys.*  
23 641 *Lipids* **2006**, *144*, 146–159.
- 24 642 (64) Niggemann, G.; Kummrow, M.; Helfrich, W. The Bending Rigidity of  
25 643 Phosphatidylcholine Bilayers: Dependences on Experimental Method, Sample Cell  
26 644 Sealing and Temperature. *J. Phys. II* **1995**, *5*, 413–425.
- 27 645 (65) Boggs, J. M. Intermolecular Hydrogen Bonding between Lipids: Influence on  
28 646 Organization and Function of Lipids in Membranes. *Can. J. Biochem.* **1980**, *58*, 755–  
29 647 770.
- 30 648 (66) Slotte, J. P. The Importance of Hydrogen Bonding in Sphingomyelin's Membrane  
31 649 Interactions with Co-Lipids. *Biochim. Biophys. Acta BBA-Biomembr.* **2016**, *1858*, 304–  
32 650 310.
- 33 651 (67) Chen, Q.; Vancso, G. J. pH Dependent Elasticity of Polystyrene-Block-Poly(acrylic  
34 652 Acid) Vesicle Shell Membranes by Atomic Force Microscopy. *Macromol. Rapid*  
35 653 *Commun.* **2011**, *32*, 1704–1709.
- 36  
37  
38  
39  
40  
41  
42  
43  
44  
45  
46  
47  
48  
49  
50  
51  
52  
53  
54  
55  
56  
57  
58  
59  
60

## 657 TABLES

658

659 Table1: Geometrical parameters of dioleoylphosphatidylcholine (DOPC) or  
660 dipalmitoylphosphatidylcholine (DPPC) liposomes and their corresponding membrane  
661 thicknesses. The height ( $H$ ) and width ( $W$ ) mean values were measured using the cross section  
662 of AFM images of the liposomes and used to calculate the volume of the adsorbed liposomes,

1  
2  
3 663 from which the mean diameter of a sphere of equivalent volume was deduced (Eq.2). The  
4  
5 664 mean values of DOPC and DPPC membrane thicknesses were measured using the jump  
6  
7  
8 665 distance  $d$  from breakthrough force curves ( $n=30$ ) recorded in PIPES/NaCl/CaCl<sub>2</sub> buffer, pH  
9  
10  
11 666 6.7 at 20°C.  
12  
13  
14

<b>Lipid</b>	<b>Mean height H of liposomes by AFM (nm)</b>	<b>Mean width W of liposomes by AFM (nm)</b>	<b>Mean diameter of equivalent sphere by AFM (nm)</b>	<b>Mean diameter of liposomes by DLS (nm)</b>	<b>Membrane thickness by AFM (nm)</b>
<b>DOPC</b>	<b>59 ± 27</b>	<b>310 ± 97</b>	<b>150 ± 90</b>	<b>120 ± 69</b>	<b>3.91 ± 0.41</b>
<b>DPPC</b>	<b>151±48</b>	<b>448 ± 154</b>	<b>296 ± 88</b>	<b>132 ±73</b>	<b>4.93 ± 0.47</b>

15  
16  
17  
18  
19  
20  
21  
22  
23  
24  
25  
26  
27  
28  
29  
30  
31  
32  
33  
34  
35  
36  
37  
38  
39 667

40  
41  
42 668  
43  
44  
45  
46  
47  
48  
49  
50  
51  
52  
53  
54  
55  
56  
57  
58  
59  
60

669

670 Table 2: Comparison of the bending modulus ( $k_C$ ) and Young modulus values ( $E$ ) of

671 liposomes or of supported lipid bilayers in the fluid or gel phase reported in the literature

672 using different techniques as indicated. Abbreviations stand for: EggPC = mixture of

673 unsaturated (54.8 wt. %) and saturated (45.2 wt. %) phosphatidylcholine; DMPC = 1,2-

674 dimyristoyl-sn-glycero-3-phosphocholine; ESM = egg sphingomyelin; Chol = cholesterol.

675 Values in italics were calculated by the authors using calculations described in the Appendix

676 (eq.A.2; A.3)

677

678

679

680

681

682

683

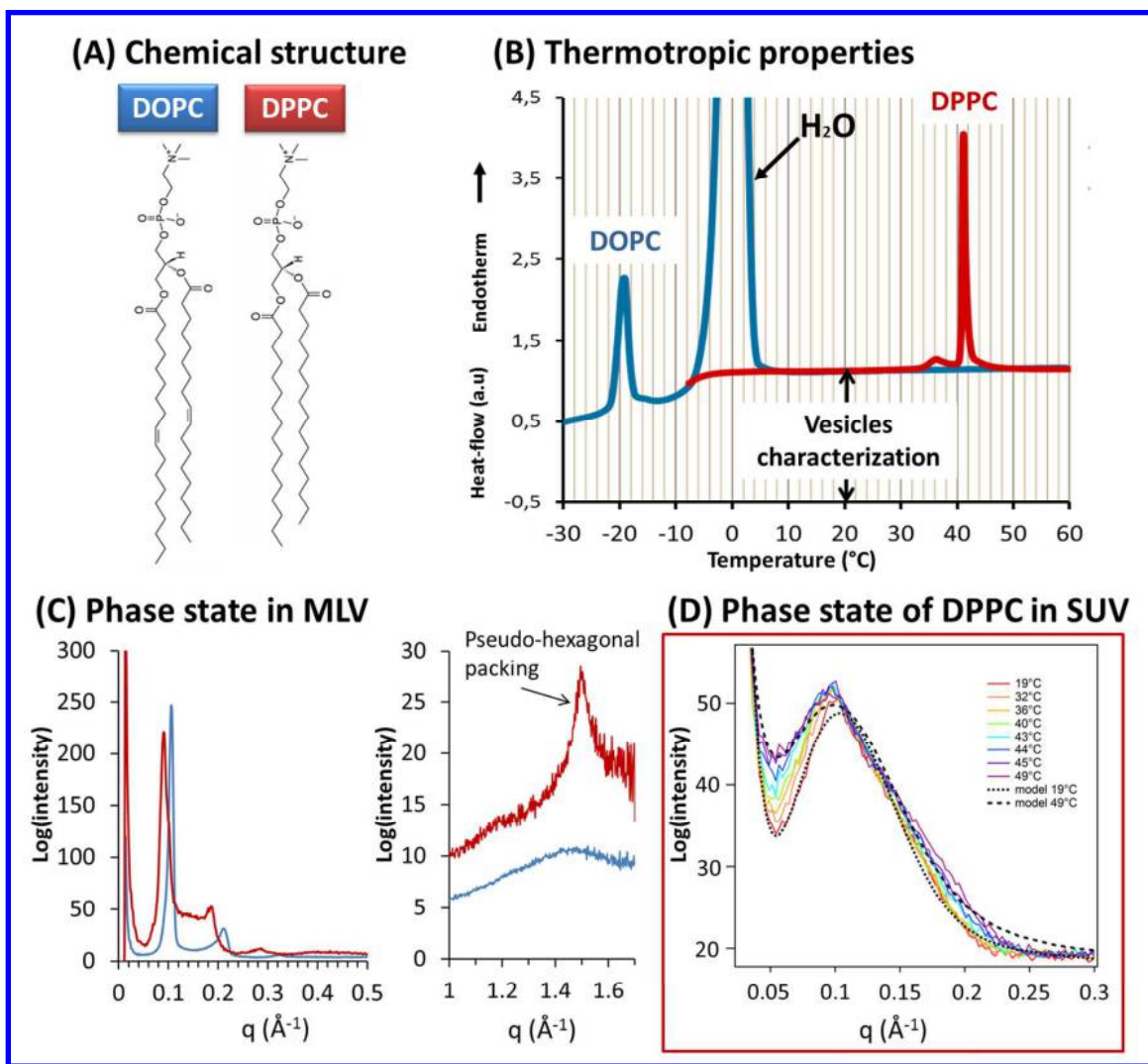
684

Reference	Lipid	Technique	Phase	Bending modulus $k_C$ ( $\times 10^{-19} \text{J}$ )	Young modulus $E$ (MPa)
<b>Liposomes (3D)</b>					
Present work	DOPC	AFM spectroscopy	Fluid	0.9	13
	DPPC	AFM spectroscopy	Gel	15.50	116
16	DPPC	AFM spectroscopy	Gel	13.54	110
21	Egg PC	AFM spectroscopy	Fluid	0.27	1.97
45	synthetic phospholipids (18:1)	Micropipette pressurization	Fluid	0.90	12.70
54	DMPC	Phase contrast microscopy	Fluid	1.27	26
55	DMPC	Phase contrast microscopy	Fluid	1.15	24
56	DOPC	Osmotic swelling	Fluid	1.06	15
<b>Supported bilayers (2D)</b>					
Present work	DOPC	AFM spectroscopy	Fluid	0.88	27
	DPPC	AFM spectroscopy	Gel	2.03	31
28	DOPC	AFM spectroscopy	Fluid	1.69	19.3
	DPPC	AFM spectroscopy	Gel	2.33	28.1
61	DOPC	AFM spectroscopy	Fluid	4.61	80
	ESM/Chol	AFM spectroscopy	Liquid ordered	12.94	140
62	DOPC	AFM spectroscopy	Fluid	8.65	150
	ESM/Chol	AFM spectroscopy	Liquid ordered	27.72	300



1  
2  
3 685  
4  
5  
6  
7 686  
8  
9  
10 687  
11  
12  
13  
14 688  
15  
16  
17 689  
18  
19  
20  
21 690  
22  
23  
24 691  
25  
26  
27  
28 692  
29  
30  
31 693  
32  
33  
34  
35  
36  
37  
38  
39  
40  
41  
42  
43  
44  
45  
46  
47  
48  
49  
50  
51  
52  
53  
54  
55  
56  
57  
58  
59  
60

694 FIGURES:



695

696

697 Figure 1: (A) Molecular structures of the unsaturated DOPC (dioleoylphosphatidylcholine)  
 698 and saturated DPPC (dipalmitoylphosphatidylcholine). (B) Differential scanning calorimetry  
 699 thermograms of DOPC (blue trace) and DPPC (red trace) multilamellar vesicles recorded on  
 700 heating at  $2^{\circ}\text{C}\cdot\text{min}^{-1}$ . (C) X-ray diffraction patterns of DOPC and DPPC fully hydrated  
 701 multilamellar vesicles recorded at  $20^{\circ}\text{C}$  at small (left) and wide (right) angles. (D) Small  
 702 angle X-ray Scattering of DPPC SUV recorded on heating. Unilamellar SAXS model at low

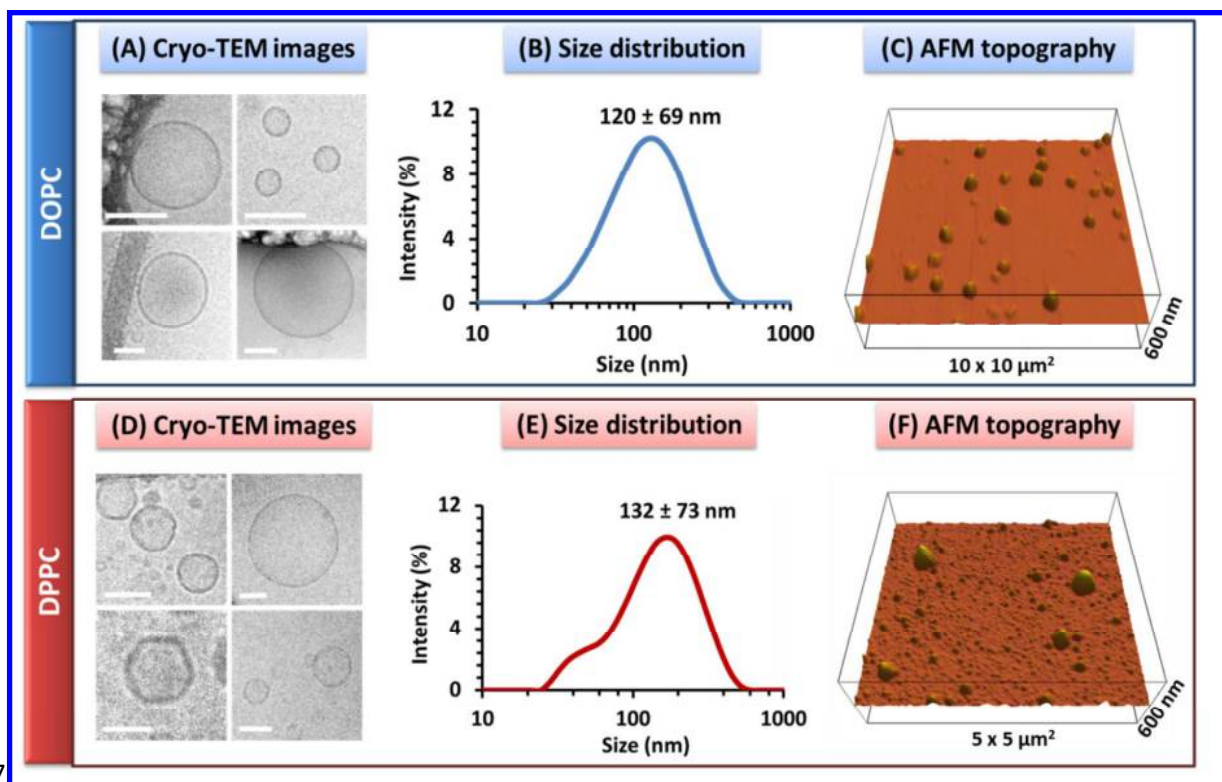
33

1  
2  
3 703 and high temperature are superimposed. All experiments were performed in aqueous  
4

5  
6 704 PIPES/NaCl/CaCl<sub>2</sub> medium at pH = 6.7.  
7

8  
9 705  
10  
11  
12  
13  
14  
15  
16  
17  
18  
19  
20  
21  
22  
23  
24  
25  
26  
27  
28  
29  
30  
31  
32  
33  
34  
35  
36  
37  
38  
39  
40  
41  
42  
43  
44  
45  
46  
47  
48  
49  
50  
51  
52  
53  
54  
55  
56  
57  
58  
59  
60

706



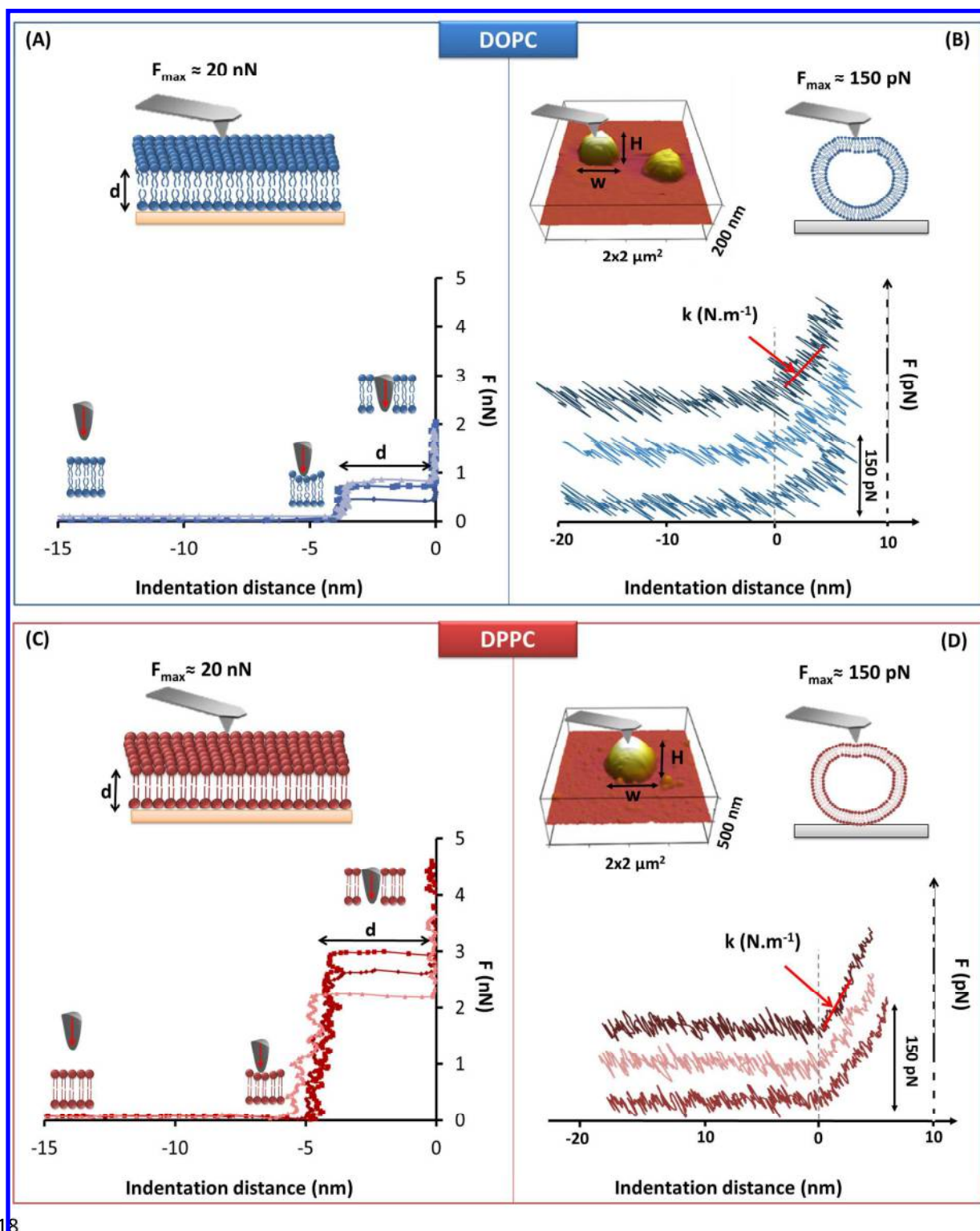
707

708 Figure 2: Characterization of the shape and size of DOPC (dioleoylphosphatidylcholine) or  
709 DPPC (dipalmitoylphosphatidylcholine) liposomes. (A) and (D) Cryo-TEM images of the  
710 DOPC and DPPC liposomes, respectively; scale bars are 100 nm. (B) and (E) Dynamic light  
711 scattering size distribution in intensity of the DOPC and DPPC liposome suspensions,  
712 respectively; and (C) and (F) typical AFM 3D images of DOPC and DPPC liposomes,  
713 respectively. All experiments were performed in aqueous PIPES/NaCl/CaCl<sub>2</sub> medium at pH =  
714 6.7 and at 20°C.

715

716

717



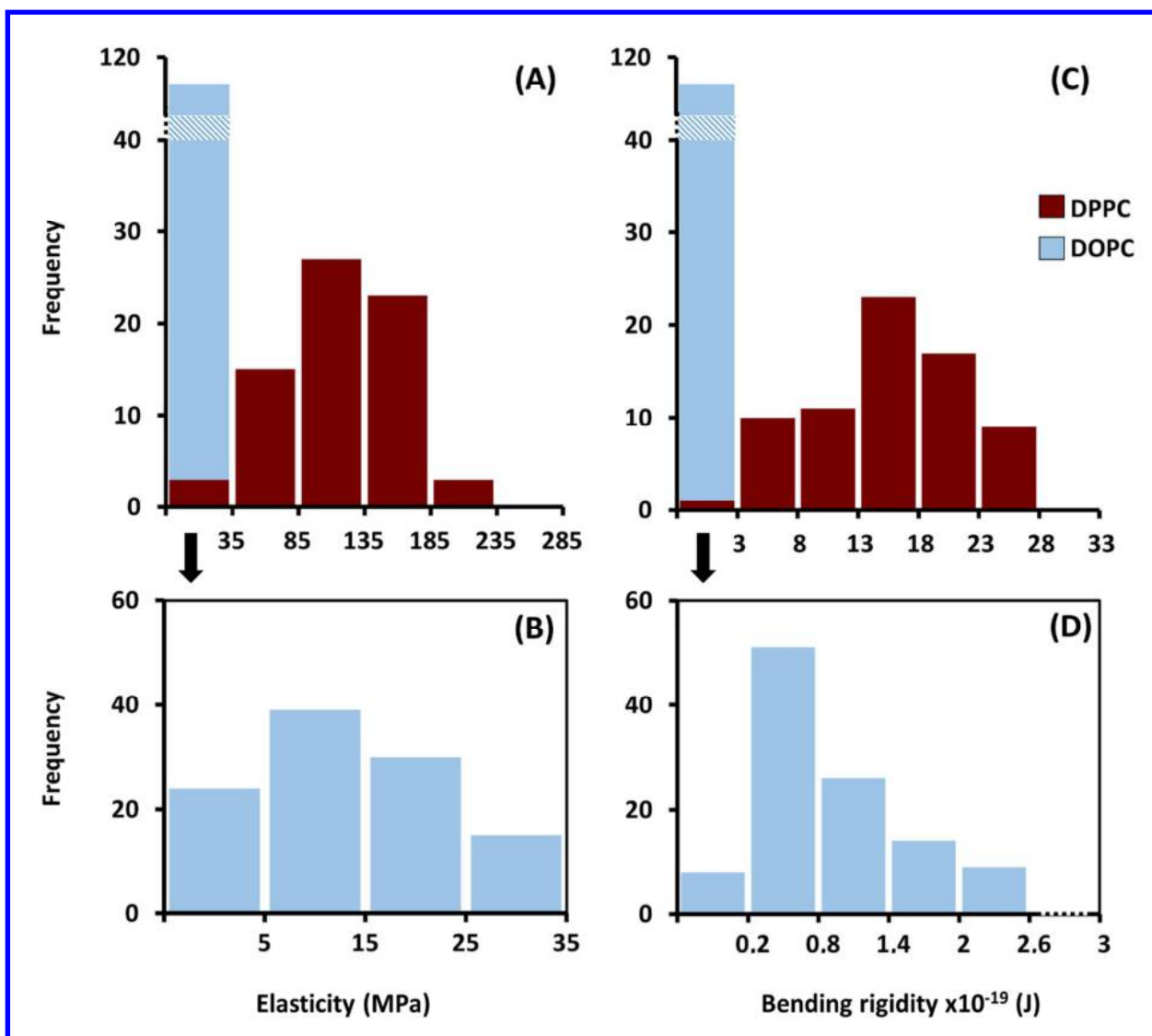
718

36

719

720 Figure 3: AFM indentation measurement on DOPC (dioleoylphosphatidylcholine, in blue) or  
721 DPPC (dipalmitoylphosphatidylcholine, in red) liposomes adsorbed on silicon substrate. (A)  
722 and (C) show the breakthrough force curves obtained as a result of tip penetration into DOPC  
723 or DPPC supported lipid bilayers, respectively. The average bilayer thickness value  $d$  was  
724 measured from the jump-through distance ( $n=50$ ). (B) and (D) show typical force curves  
725 acquired during indentation of, respectively, DOPC or DPPC liposomes in the elastic regime;  
726 in order to infer the bilayer stiffness  $k$  from the slope after tip-membrane contact. For the sake  
727 of clarity, the force curves are shifted along the Y axis. All measurements were recorded in  
728 aqueous PIPES/NaCl/CaCl<sub>2</sub> medium at pH = 6.7 and at 20°C.

729



730

731

732

733

734 Figure 4: Distributions of the Young moduli  $E$  and of the bending rigidity  $k_C$ , independent of735 liposome size, of DOPC ( $n=108$ ) and DPPC ( $n=71$ ). (A) and (C) show the superposition of736 both DOPC and DPPC frequency distributions for  $E$  and  $k_C$ , respectively. (B) and (D) show

1  
2  
3 737 respective enlargements of the  $E$  and  $k_C$  frequency distributions for the DOPC liposomes. All  
4  
5  
6 738 measurements were recorded in aqueous PIPES/NaCl/CaCl<sub>2</sub> medium at pH = 6.7 and at 20°C.  
7  
8  
9 739  
10  
11  
12 740  
13  
14  
15  
16  
17  
18  
19  
20  
21  
22  
23  
24  
25  
26  
27  
28  
29  
30  
31  
32  
33  
34  
35  
36  
37  
38  
39  
40  
41  
42  
43  
44  
45  
46  
47  
48  
49  
50  
51  
52  
53  
54  
55  
56  
57  
58  
59  
60



741 **Table of contents graphic**

742

743

744

